

Mn₂CoZ (Z=Al, Ga, In, Si, Ge, Sn, Sb) compounds: Structural, electronic, and magnetic properties

G. D. Liu,¹ X. F. Dai,² H. Y. Liu,² J. L. Chen,¹ Y. X. Li,² Gang Xiao,³ and G. H. Wu¹

¹Beijing National Laboratory for Condensed Matter Physics, Institute of Physics, Chinese Academy of Sciences, Beijing 100080, People's Republic of China

²School of Material Sciences and Engineering, Hebei University of Technology, Tianjin 300130, People's Republic of China

³Department of Physics, Brown University, Providence, Rhode Island 02912, USA

(Received 4 April 2007; published 17 January 2008)

We study the electronic structures and magnetic properties of Mn₂CoZ (Z=Al, Ga, In, Si, Ge, Sn, Sb) compounds with Hg₂CuTi-type structure using first-principles full-potential linearized-augmented plane-wave calculations. It is found that the compounds with Z=Al, Si, Ge, Sn, and Sb are half-metallic ferrimagnet. Experimentally, we successfully synthesized the Mn₂CoZ (Z=Al, Ga, In, Ge, Sn, Sb) compounds. Using the x-ray diffraction method and Rietveld refinement, we confirm that these compounds form Hg₂CuTi-type structure instead of the conventional L2₁ structure. Based on the analysis on the electronic structures, we find that there are two mechanisms to induce the minority-spin band gap near the Fermi level, but only the *d-d* band gap determines the final width of the band gap. The magnetic interaction is quite complex in these alloys. It is the hybridization between the Mn(*C*) and Co atom that dominates the magnitude of magnetic moment of the Co atom and the sign of the Mn(*B*)-Co exchange interaction. The Mn₂CoZ alloys follow the Slater-Pauling rule $M_H = N_V - 24$ with varying Z atom. It was further elucidated that the molecular magnetic moment M_H increases with increasing valence concentration only by decreasing the antiparallel magnetic moment of Mn(*C*), while the magnetic moments of Mn(*B*) and Co are unaffected.

DOI: 10.1103/PhysRevB.77.014424

PACS number(s): 75.50.Cc, 71.20.Lp

I. INTRODUCTION

Half-metallic materials¹ exhibiting a complete spin polarization ($P=100\%$) at the Fermi surface have received growing interest due to its great value for spintronic devices such as nonvolatile magnetic random access memories and magnetic sensors.² Especially, the half-metallic materials with low spin magnetic moments seem to be highly desirable for realistic applications since they lead to smaller energy losses due to the lower external magnetic fields created with respect to their ferromagnetic counterparts.³ After the pioneering work of von Leuken and de Groot,⁴ the concept of half-metallic ferrimagnetism and antiferromagnetism received considerable theoretical interest. Pickett⁵ and Park *et al.*⁶ searched for and investigated the half-metallic antiferromagnetic double-perovskite-structure oxides based on the theoretical exploration of electronic structures. Akai and Ogura reported the possibility of half-metallic antiferromagnetism in the diluted magnetic semiconductors on the basis of the first-principles electronic structure calculation.⁷

In fact, more investigations on the half-metallic materials were focused on the Heusler alloy system. It is well known that a number of Heusler alloys⁸ have been predicted based on first-principles calculations to be half-metallic. Some alloys, e.g., XMnSb (X=Ni, Co, etc.),^{1,9} Co₂MnZ (Z=Si, Ga, Ge, Sn),¹⁰⁻¹⁴ and Mn₂VZ (Z=Al, Ga, Si, etc.),¹⁵⁻¹⁸ have been investigated experimentally in detail on their structural, electronic, and magnetic properties in the past two decades. Recently, Ozdogan *et al.* reported the defect-driven appearance of half-metallic ferrimagnetism in Co-Mn-based Heusler alloys³ and the defect-induced ferrimagnetism in the half-metallic Co₂CrAl and Co₂CrSi compounds.¹⁹ Galanakis *et al.* investigated the half-metallic antiferromagnetism of the

doped Mn₂VAl and Mn₂VSi Heusler alloys.²⁰ Increasing evidence has indicated that Heusler-type alloys is a promising set of compounds to search for new half-metallic materials.

Heusler alloys are represented in general by the generic formula X₂YZ, where X and Y denote some transition-metal elements and Z an *s-p* element.^{21,22} Usually, the ternary compounds have a highly ordered L2₁ structure, which belongs to the $Fm\bar{3}m$ space group. The structure's prototype is the Cu₂MnAl alloy. In past studies, the most Mn-contained Heusler alloys only have one Mn atom per f.u. with the Mn atom occupying the Y site in the L2₁ structure. Few alloys containing two Mn atoms per f.u. were investigated, among which are the Mn₂V-based compounds that are of the L2₁ structure.¹⁵⁻²¹ However, the Mn₂NiSn forms the Hg₂CuTi-type structure,²³ which is different from the conventional Heusler alloys. Its space group is $F\bar{4}3m$, the same as that of the semi-Heusler alloy.

Recently, we reported that the Mn₂NiGa and Mn₂CoSb alloys prefer to form the Hg₂CuTi-type structure.^{24,25} The two Mn atoms as nearest neighbors to each other bring about a quite complex magnetic interaction, which lead to a series of physical properties for the Mn₂Co-based alloys. For example, Mn₂CoSb's half-metallicity²⁵ is a result of the Hg₂CuTi-type structure. Mn₂CoZ is a potential class of Heusler alloys with half-metallicity.

In this work, we present a study on a series of Mn₂CoZ alloys (Z=Al, Ga, In, Si, Ge, Sn, and Sb). Most of them except Z=Si have been synthesized and structurally characterized, as will be described later. We have determined that these compounds are of the Hg₂CuTi-type structure instead of the conventional L2₁ structure. Most interestingly, our first-principles calculations have predicted that the com-

TABLE I. The fabrication method, lattice constant, calculated band gap, and spin-flip gap (HM gap) for Mn_2CoZ ($Z=\text{Al, Ga, In, Si, Ge, Sn, Sb}$) compounds. The symbol “*” indicates that the lattice constant is hypothetical and the other was obtained by experimental results.

Compostion Mn_2CoZ	Fabrication method	Lattice constant (Å)	Band gap (eV)	HM gap (eV)
Al	Arc melt	5.8388	0.2245	0.016
Ga	Arc melt	5.8620	0.05	-0.100
In	Arc melt	6.1420		
Si		5.8000*	0.3971	0.188
Ge	Annealing	5.8000	0.2692	0.100
Sn	Melt spun	6.0588	0.09410	0.070
Sb	Melt spun	5.9042	0.4004	0.134
Sn		5.8000*	0.2291	0.050

pounds with $Z=\text{Al, Si, Ge, Sn, and Sb}$ are half-metallic material with ferrimagnetism. We will discuss the formation of half-metallicity and the magnetic properties of these alloys in detail. We will show that there are two mechanisms to induce the minority-spin band gap near the Fermi level, but only the $d-d$ band gap determines the final width of the band gap. It is the hybridization between the Mn(C) and Co atom that dominates the magnitude of magnetic moment of the Co atom and the sign of the Mn(B)-Co exchange interaction. We will also show that the Mn_2CoZ alloys follow the Slater-Pauling rule $M_H=N_V-24$ with varying Z . We will elucidate that the molecular magnetic moment M_H increases with increasing valence concentration only by the reduction of the antiparallel magnetic moment of Mn(C), while the magnetic moments of Mn(B) and Co remain primarily unchanged.

II. EXPERIMENTAL AND COMPUTATIONAL DETAILS

Not all the Mn_2CoZ alloys with different Z elements can be synthesized to a pure body-centered cubic (bcc) structure by using the arc-melt method. We have used both the arc-melt and the melt-spun techniques with appropriate annealing process to fabricate Mn_2CoZ alloys with pure bcc structure. Initially, we prepared all precursor ingots with relevant components and compositions by arc melting pure metals in the argon atmosphere. If necessary, some precursor ingots were melt spun into ribbons with widths of 2–3 mm and thicknesses of 40–50 μm at a linear velocity of 12 m/s; other precursor ingots were encapsulated under argon in quartz glass and annealed at 1073 K for 72 h. Table I lists preparation methods and various parameters for all samples fabricated. We analyzed the structure of all the samples using powder x-ray diffraction (XRD) ($\text{Cu } K\alpha$) and Rietveld refinement methods. We measured the magnetization of these samples using a superconducting quantum interference device magnetometer in fields up to 5 T at 5 K.

Based on the structure and the experimentally determined lattice constants of the fabricated alloys, we calculated the

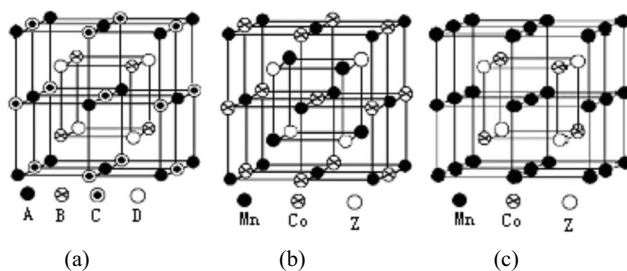


FIG. 1. (a) The generalized Heusler structure with four interpenetrating fcc sublattices $A, B, C,$ and D . The structure models of Mn_2CoZ : (b) the Hg_2CuTi -type structure and (c) the conventional $L2_1$ structure.

electronic structure of the materials using the self-consistent full-potential linearized-augmented plane-wave (FLAPW) method based on the local density approximation within the density functional theory.^{26,27} Fifty k points in the irreducible Brillouin zone were used to achieve the self-consistency in the calculation. The self-consistency is better than 0.01 me/a.u. for charge density and spin density and the stability is better than 0.1 mRy for the total energy per cell. The muffin-tin sphere radii R were chosen as $R_{\text{Al}}=2.5$ a.u., $R_{\text{Si}}=2.1$, $R_{\text{Sb}}=2.6$ a.u., $R_{\text{Ga}}=R_{\text{In}}=R_{\text{Ge}}=R_{\text{Sn}}=2.3$ a.u., and $R_{\text{Mn}}=R_{\text{Co}}=2.2$ a.u. The density plane-wave cutoff is $Rk_{\text{max}}=8.0$. The electron states were treated in a scalar relativistic approximation. Using the energy eigenvalues and eigenvectors at these points, the density of states was determined by the tetrahedral integration method.^{28,29}

III. RESULTS AND DISCUSSIONS

A. Crystal structure

In our previous work, we have reported that Mn_2NiGa and Mn_2CoSb form the Hg_2CuTi -type structure,^{1,24,25} whose structural model is shown in Fig. 1. The main difference from the conventional Heusler alloys with Cu_2MnAl -type or Hg_2Ti -type structures yield two types of superlattice reflections superposed onto the fundamental diffraction pattern. The diffraction peaks for the (h, k, l) planes can be categorized as follows: a type I superlattice reflection when h, k, l are all odd [e.g., (111) peak], a type II superlattice reflection when h, k, l are all even and $h+k+l=2n$ [e.g., (200) peak], and fundamental reflections where h, k, l are all even and $h+k+l=4n$ [e.g., (220) peak].^{21,30}

For materials with these structures, the structure factors $F(111)$ and $F(200)$ correspond to the order-dependent superlattice reflections, while $F(220)$ corresponds to order-independent principal reflections. Therefore, the ratio of the superlattice intensity to the principal peak intensity provides information on the antisite disorder in the following ways: (1) disorder between B and D sublattices reduces the type I superlattice peak to zero in the limit of complete disorder and (2) disorder between the $A, C,$ and B superlattices reduces the intensities of type II superlattice peaks relative to that of the principal reflections.³⁰

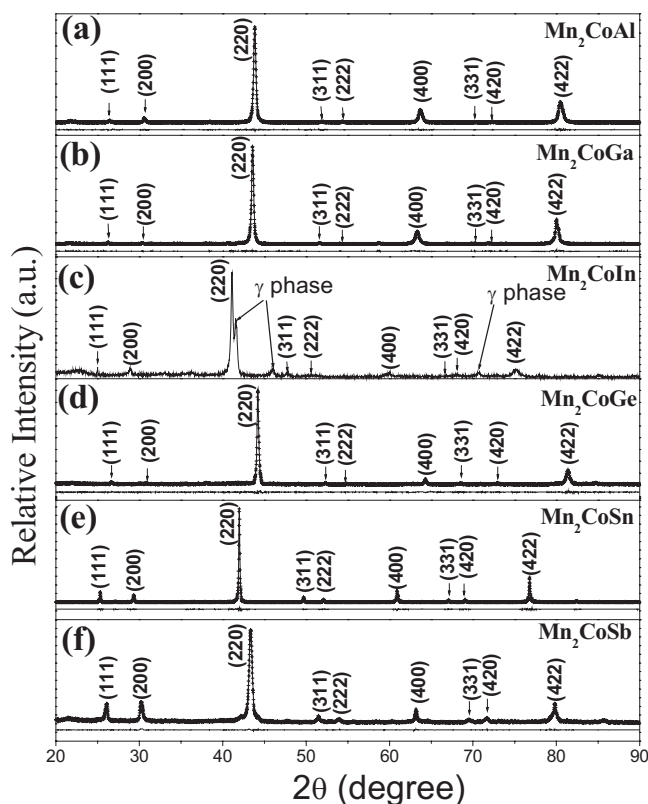


FIG. 2. X-ray diffraction patterns of Mn₂CoZ (Z = Al, Ga, In, Ge, Sn, Sb) alloys: experimental data (+) for the powder samples and calculated data (continuous line) for the Hg₂CuTi-type model. The bottom curve shows the difference between experimental and calculated data on the same scale as the diffraction.

The experimental XRD patterns for powdered Mn₂CoZ (Z=Al, Ga, In, Ge, Sn, Sb) are shown in Fig. 2. For the Mn₂CoZ (Z=Al, Ga, Ge, Sn, Sb) alloys, all the principal reflection peaks of bcc structure are observed without the other secondary peaks on the XRD patterns, indicating that the Mn₂CoZ form the pure bcc structure. Furthermore, it is noted that all the XRD patterns for Mn₂CoZ alloys with bcc structure display the (111) and (200) peaks, which strongly suggests that a highly ordered Hg₂CuTi-type structure has been formed in these alloys. The Rietveld refinement analyses were carried out to identify the degree of atomic ordering in these alloys. Using the Hg₂CuTi-type model, the Rietveld refinement results are also shown in Fig. 2. It is clear that the observed XRD patterns match the refinement results very well. We also used the Cu₂MnAl-type model to refine the experimental data and the results show a worse fit than that using the Hg₂CuTi-type model, which is similar to the case in Mn₂NiGa and Mn₂NiSn.^{23,24}

In the Mn₂CoIn alloy, there is a small amount of second phase (γ phase with fcc structure) embedded in the main bcc structure, as seen in the XRD pattern of Fig. 2(c). The (111) and (200) superlattice peaks can still be observed in the XRD pattern of the Mn₂CoIn alloys though the experimental intensity of the (111) peak is slightly weaker than the calculated value. As mentioned earlier, the weakness of the (111) peak

can be attributed to the small antisite disordering between Mn(C) and In. For Z=Si, we were not able to form the bcc structure using whatever method.

Burch *et al.* showed that in the Fe₃Si compound (the Fe₃Si can be considered as Fe₂FeSi with a Heusler structure), partly substituting transition metals (as impurities) for Fe reveals a noticeable preference of occupation of one type of Fe site depending on the number of 3d electrons. Transition-metal impurities on the left-hand side of Fe in the Periodic Table (e.g., Mn or V) demonstrate strong preference for B site occupation, whereas atoms on the right side of Fe (e.g., Co) prefer (A, C) sites.^{31,32}

For the Mn₂YZ compounds, we also observed a rule similar to that reported by Burch *et al.* We have observed that if Y elements are Ni or Co (on the right-hand side of Mn), they prefer to occupy the (A, C) sites in Mn₂Ni- and Mn₂Co-based compounds and be crystallized in the Hg₂CuTi-type structure. When the Y atom is V (on the left-hand side element of Mn), it shows a strong preference for B site occupation in Mn₂V-based alloys and is crystallized in conventional Cu₂MnAl-type structure.¹¹⁻¹⁴ Based on this rule, it is easy to estimate the superlattice structure of the Heusler-like compounds. Furthermore, we can also consider the rule to be fit to the quaternary alloys. In addition, the selectivity of occupation for our materials is also supported by the first-principles total energy calculations, which will be reported elsewhere. So, we believe that our Mn₂CoZ alloys formed the Hg₂CuTi-type structure.

B. General discussion on electronic structure

The lattice parameters of Mn₂CoZ obtained experimentally were shown in Table I. One exception is the lattice parameter for Mn₂CoSi, which we assumed to be 5.80 Å, the same as that of Mn₂CoGe, as we have not experimentally synthesized the alloy. The Hg₂TiCu-type model with ideal occupation of elements was used to carry out the first-principles calculation. In addition, to separate the influence of the lattice constant and the binding energy of *p* electrons, we also show the related data in Table I for the Mn₂CoSn compound with the lattice of 5.80 Å, which is smaller than the experimental result but equal to that of Mn₂CoZ (Z = Si, Ge).

Figures 3-5 display the band structures of Mn₂CoZ compounds with Hg₂TiCu-type structure for the spin-up (majority) and the spin-down (minority) electrons. It is evident that the majority band structure has metallic intersections for all compounds at the Fermi level, indicating a strong metallic nature of the majority electrons. However, the minority band structure of these alloys exhibits a band gap near the Fermi level except for Mn₂CoIn. Therefore, our calculation reveals that Mn₂CoZ (Z=Al, Si, Ge, Sn, and Sb) alloys may form another family of half-metals. For the alloys with Z=Ga, the minority valence band maximum is only slightly above the Fermi level, yielding a rather small density of states at the Fermi level. For the alloys with Z=In, the Fermi level falls into a deep valley and there are a little density of states at the Fermi level. Alloys with Z=Ga and In may exhibit weakened half-metallic properties.

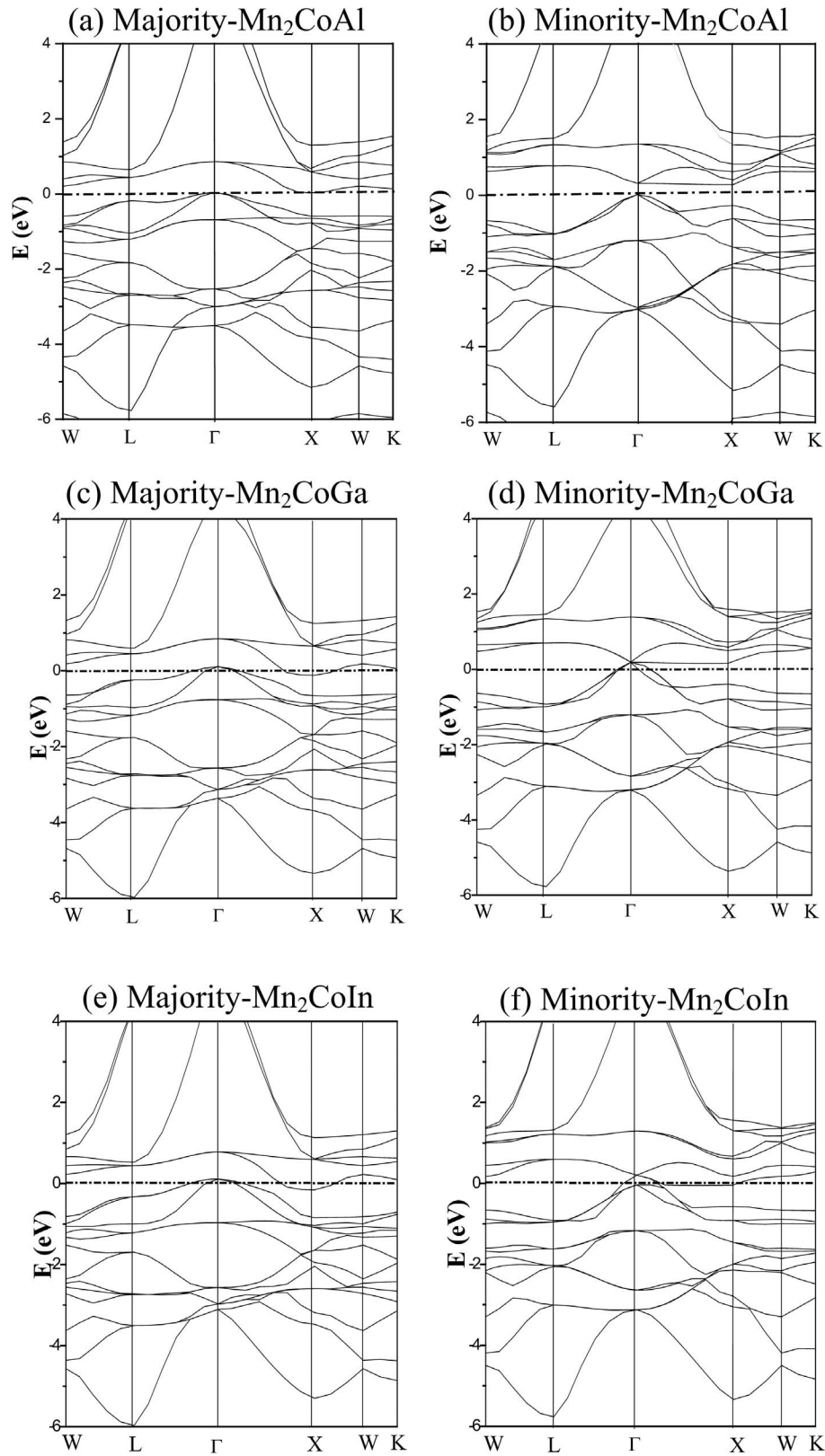


FIG. 3. Majority-spin (left column) and minority-spin (right column) band structures for Mn_2CoZ ($Z=\text{Al}, \text{Ga}, \text{In}$) alloys at the experimental lattice constants of 5.8388, 5.8620, and 6.1420 Å, respectively.

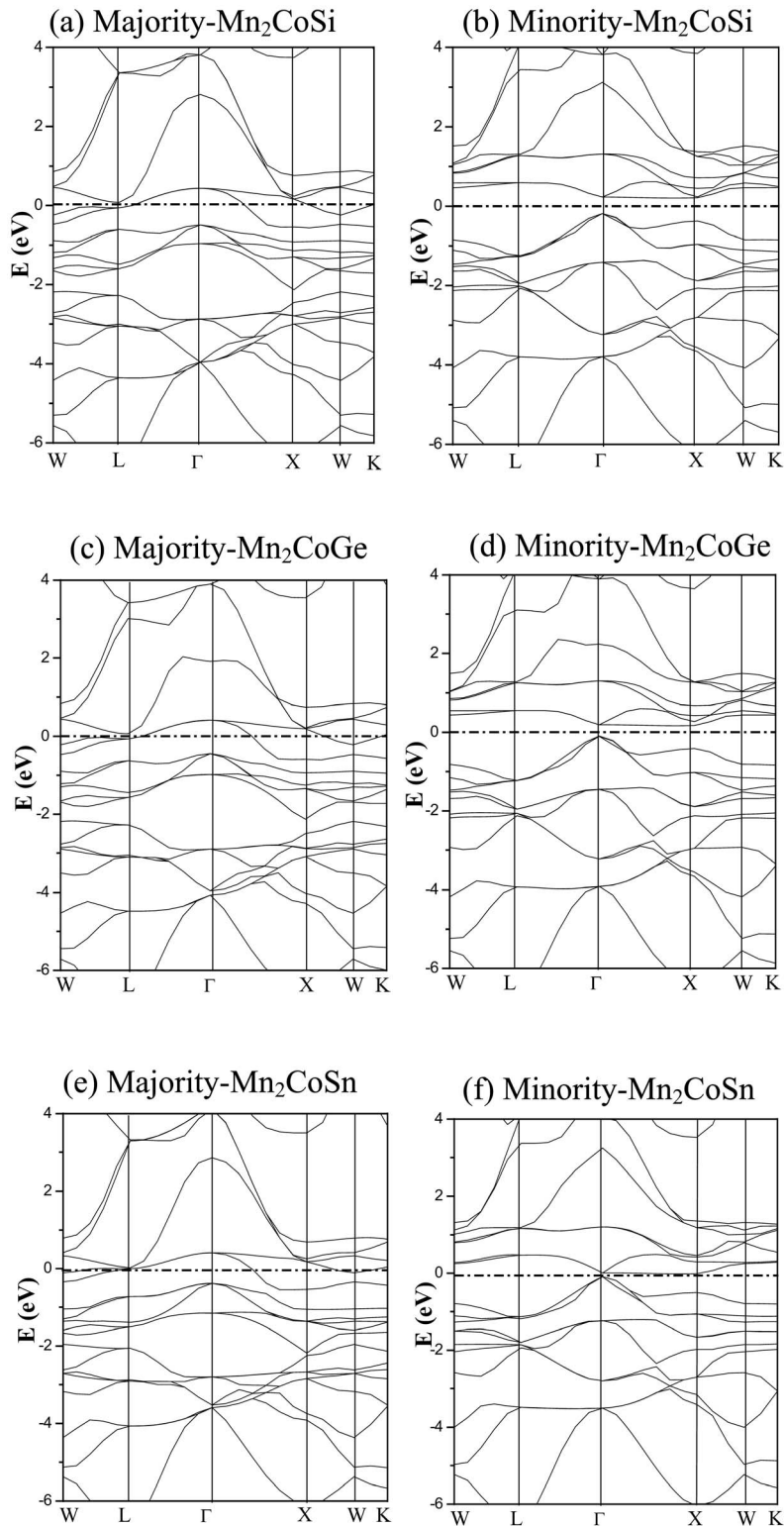


FIG. 4. Majority-spin (left column) and minority-spin (right column) band structures for Mn₂CoSi at the hypothetic lattice constant of 5.80 Å and Mn₂CoZ (Z=Ge, Sn) alloys at the experimental lattice constants of 5.80 and 6.042 Å, respectively.

With the help of the density of states (DOS), as shown in Figs. 6–12, it is clear that the energy regions of -7 to -10 eV (for Z=Al, Ga, In), -9.5 to -12 eV (for Si, Ge, Sn), and -10.5 to -13.5 eV (for Sb) consist mainly of s electrons

of the Z atoms ($4s$ or $5s$) and the band structure is almost identical for both spin directions. These lowest valence bands are separated from the other valence bands by an energy gap for both majority and minority spins and unaffected

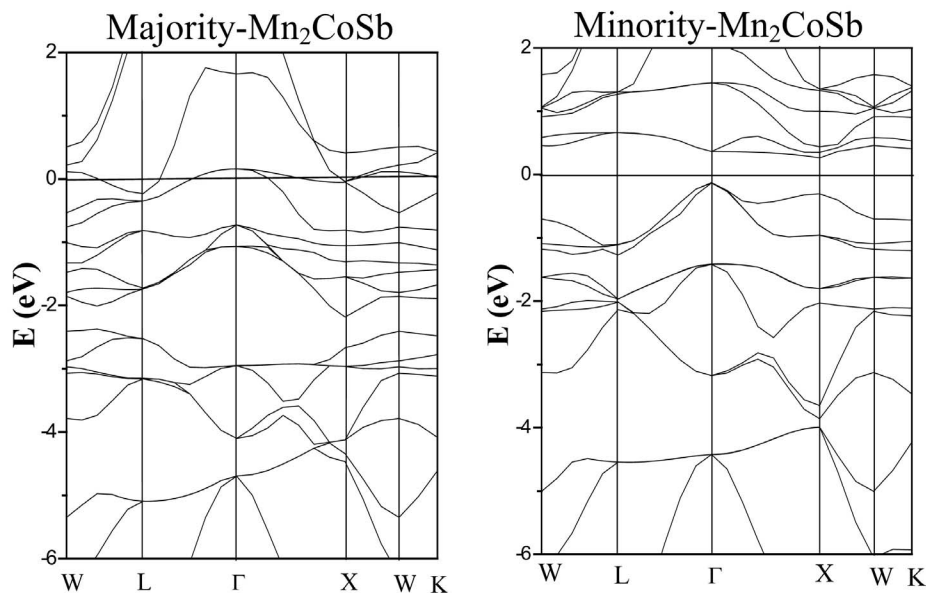


FIG. 5. Majority-spin (left column) and minority-spin (right column) band structures for Mn_2CoSb alloy at the experimental lattice constant of 5.8620 Å.

by the Co-Mn or Mn-Mn exchange interaction. Therefore, the s electrons have little influence on the magnetic moment and the formation of a half-metallic band gap, except extending the valence to a broader range. We did not show these s bands in the band graphs of Fig. 3–5. The energy region between -7 and 0 eV consists mainly of the d electrons of Co and Mn atoms. These dispersed bands are due to the strong hybridization of Mn-Mn and Mn-Co d electrons, including a contribution from Zp states in the occupied valence states.

From the total DOS, as shown in Figs. 6–12, one can see that the shape of all the density of states is similar except for some detailed difference. For the majority-spin states, there appear to be three peaks. The two peaks at the lower energies can be traced to the e_g-t_{2g} splitting in the cubic crystal field, and the peak at the higher energy is composed of antibonding d bands of mostly Mn(C) character. For the minority-spin states, two main peaks can be observed. The peak at about 1.3 eV above Fermi level is of an antibonding nature mainly arising from the Mn(B) atom.

The covalent hybridization between the lower-energy d states of the high-valent transition-metal atom such as Ni or Co and the higher-energy d states of the lower-valent transition metal can lead to the formation of bonding and antibonding bands. The bonding hybrids are localized mainly at the high-valent transition-metal atom site, while the unoccupied antibonding states are localized mainly at the lower-valent transition-metal site.⁴ In order to reveal the situation more clearly, we also show the partial DOS (PDOS) for the d component for Co, Mn(B), and Mn(C) atoms and s , p components for the Z atoms in Figs. 6–12. It is clear that there are strong hybridizations between the transition-metal atoms. The bonding states are mainly localized at the Co site, while the antibonding states are localized at the Mn(B) site for majority-spin states and at the Mn(C) site for minority-spin states.

In addition, the p electrons of the $s-p$ element also hybridize with the d states, which determine the degree of occupation of the $p-d$ orbitals. We should note that the energy of the p electrons is strongly dependent on Z atoms, which can be clearly seen in the PDOS patterns. The hybridization between p electrons with different energies and d electrons is crucial to the width of the energy gap in the minority-spin band, as will be illustrated below.

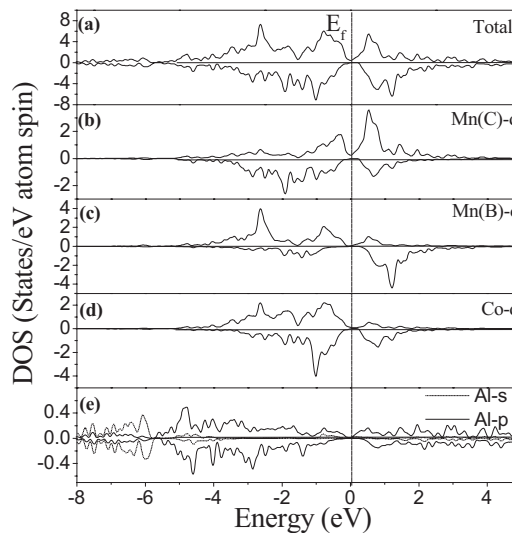


FIG. 6. Calculated spin-projected DOS plots for Mn_2CoAl at the experimental lattice constant of 5.8388 Å. (a) The total DOS of Mn_2CoAl , (b) the partial DOS of the d component of Mn(C) atoms, (c) the partial DOS of the d component of Mn(B) atoms, (d) the partial DOS of the d component of Co atoms, and (e) the partial DOS of s and p components of Al atoms. The upper halves of each panel display the spin-up states and the lower halves the spin-down states.

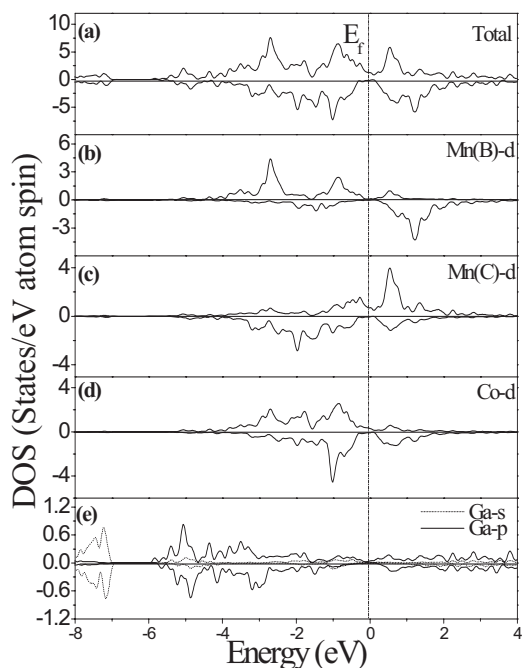


FIG. 7. Calculated spin-projected DOS plots for cubic Mn₂CoGa at the lattice constant of 5.8620 Å. (a) The total DOS of Mn₂CoGa, (b) the partial DOS of the *d* component of Mn(C) atoms, (c) the partial DOS of the *d* component of Mn(B) atoms, (d) the partial DOS of the *d* component of Co atoms, and (e) the partial DOS of *s* and *p* components of Ga atoms. The upper halves of each panel display the spin-up states and the lower halves the spin-down states.

C. Origin of the band gap

In this section, we will focus on the energy gap in minority-spin states. Such a gap is the most important feature of a half-metal. In the alloys with composition of $Z=\text{Al, Ga, Si, Ge, Sn, and Sb}$, the calculated results show an indirect Γ - X band gap for the minority carriers, as shown in Figs. 3–5. The detailed data are listed in Table I. The origin of the band gap is usually distinguished into three categories: (1) covalent band gap, (2) *d-d* band gap, and (3) charge transfer band gap.³³ The covalent band gap has been shown to exist in semi-Heusler alloys with $C1_b$ structure (e.g., NiMnSb). The *d-d* band gap is responsible for the half-metallicity of the full-Heusler alloys with $L2_1$ structure (e.g., Mn₂VAl). The charge transfer band gap is usually common in CrO₂ and double perovskites.

In our Mn₂CoZ alloys, the situation is more complex due to the special crystallized structure (as shown in Sec. III A). The Mn₂CoZ alloys have a space group similar to the semi-Heusler CoMnZ alloys but the empty site was alternated by the additional Mn atom. Compared with the full-Heusler alloy with $L2_1$ structure (Mn₂VAl), the Mn atoms occupy two sublattices with different surroundings in Mn₂CoZ alloys. Therefore, we must pay attention to the effects of these two Mn atoms.

To understand the origin of the band gap, let us observe again the PDOS shown in Figs. 6–12. First, we focus on the Mn(B) atom. It can be seen that all of the Mn(B) atoms in

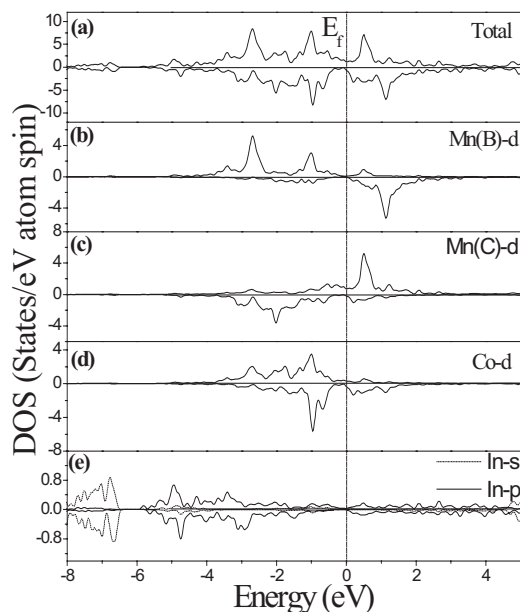


FIG. 8. Calculated spin-projected DOS plots for Mn₂CoIn with the experimental lattice constant of 6.140 Å. (a) The total DOS of Mn₂CoIn, (b) the partial DOS of the *d* component of Mn(B) atoms, (c) the partial DOS of the *d* component of Mn(C) atoms, (d) the partial DOS of the *d* component of Co atoms, and (e) the partial DOS of *s* and *p* components of In atoms. The upper halves of each panel display the spin-up states and the lower halves the spin-down states.

the Mn₂CoZ alloys have the similar feature of DOS. The minority-spin band structure can be characterized by the large band gap near the Fermi level and the unoccupied antibonding bands at higher energies. Mn(C) and Co atoms are the nearest neighbors of Mn(B). As mentioned in Sec. III B, there is a strong covalent hybridization between the *d* states of Mn(C), Co, and Mn(B), which leads to the formation of the bonding and antibonding bands separated by the gap. Therefore, the gap in the minority-spin states of Mn(B) arises primarily from the covalent hybridization similar to semi-Heusler half-metal alloys (e.g., NiMnSb and CoMnSb).⁹

For Mn(C) and Co atoms, the situation is very different from the Mn(B) atom. They have a similar gap width, while the Mn(B) atom has a larger gap width. Hence, the actual gap width in the Mn₂CoZ compounds is determined mainly by the Mn(C) and Co atoms. Furthermore, it can be understood that it is the tail of the *d* states of the Mn(C) and Co hybridized with Zp states that determines the character of the minority-spin gap. Obviously, the highest occupied minority states mainly consist of *d* states of Mn(C) and Co atoms. Also, there is a peak at about 0.5 eV above the Fermi level in the minority-spin states of the Mn(C) and Co atoms, which is lower than the antibonding peak of Mn(B) and only has a small overlap with the antibonding states of Mn(B) in energy, indicating that a hybridization only occurs between Mn(C) and Co. Therefore, it may be reasonable to consider first the interactions between the Mn(C) atom and the Co atom and then the interaction with the Mn(B) or the *s-p*

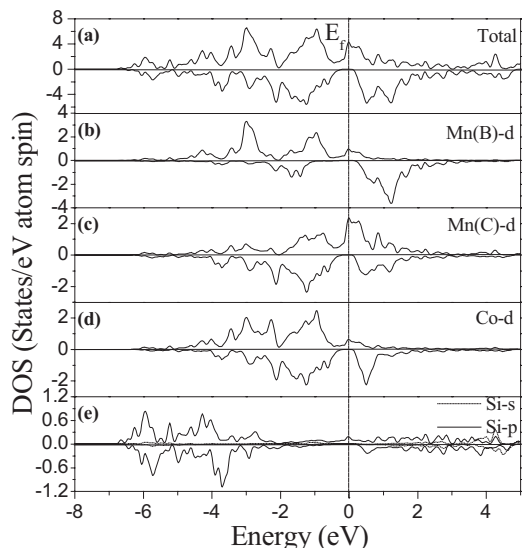


FIG. 9. Calculated spin-projected DOS plots for Mn_2CoSi with the hypothetical lattice constant of 5.800 Å. (a) The total DOS of Mn_2CoSi , (b) the partial DOS of the d component of Mn(B) atoms, (c) the partial DOS of the d component of Mn(C) atoms, (d) the partial DOS of the d component of Co atoms, and (e) the partial DOS of s and p components of Si atoms. The upper halves of each panel display the spin-up states and the lower halves the spin-down states.

atom, as was also the case for the Co_2MnZ (Ref. 34) and Fe_2MnZ .³⁵

The Heusler alloy has a tetrahedral T_d symmetry. However, if we neglect the B and D sites, the lattice consisting of only A and C sites has the O_h symmetry. T_d is a subgroup of O_h . Thus, it is possible to have states located only at the A and C sites as there are no states at the B site with the same representation. Based on these, Galanakis *et al.* successfully explained the origin of the band gap of Co_2MnZ alloys. The situation in our Mn_2CoZ alloys is quite similar to that in Co_2MnZ . The possible hybridization between spin-down orbitals sitting at the different sites in the case of our Mn_2CoZ alloys will create several energy levels: e_g , t_{2g} , e_u , and t_{1u} . The exchange splitting will shift the Fermi level to the appropriate position. As elucidated above, the states at two edges of the band gap is mainly of Mn(C) and Co characters instead of Mn(B) ones. So, as in the Co_2MnZ alloy, the states can be well ascribed to the doubly degenerated e_u state and triply degenerated t_{1u} state, which only arise from the hybridization with Mn(C) and Co d states.³⁴ The e_u and t_{1u} orbitals cannot couple with any of the Mn(B) d orbitals as the Mn(B) d orbitals do not transform with the u representations. Furthermore, we point out that the t_{1u} states are below the Fermi level, while the e_u states are just above the Fermi level due to the fact that the total eight minority d bands are filled in our Mn_2CoZ compounds. So, it is clear that the band gap of the Mn(C) and Co atom is the d - d band gap, and it arises only from the e_u - t_{1u} splitting instead of the conventional e_g - t_{2g} one in Heusler alloys.

The Mn(C) and Co atoms are the second nearest neighbors; therefore, the e_u - t_{1u} splitting is weak and leads to a

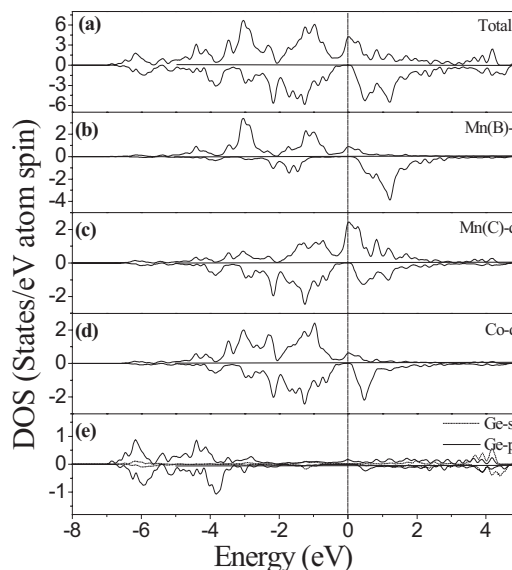


FIG. 10. Calculated spin-projected DOS plots for Mn_2CoGe with the experimental lattice constant of 5.80 Å. (a) The total DOS of Mn_2CoGe , (b) the partial DOS of the d component of Mn(B) atoms, (c) the partial DOS of the d component of Mn(C) atoms, (d) the partial DOS of the d component of Ni atoms, and (e) the partial DOS of s and p components of Ge atoms. The upper halves of each panel display the spin-up states and the lower halves the spin-down states.

smaller gap than that of the Mn(B) atom. In conclusion, it should be emphasized that there exist two mechanisms in the formation of the band gap in the Mn_2CoZ compounds, that is, covalent band gap and d - d band gap, but it is mainly the d - d band gap that characterizes the half-metallicity in Mn_2CoZ alloys.

From Table I, we can also find that the width of the energy gap decreases with increasing atomic number in a group of the Periodic Table (e.g., Si \rightarrow Ge \rightarrow Sn) but increases in a row (e.g., In \rightarrow Sn \rightarrow Sb), which is also observed in the full-Heusler alloy Co_2MnZ ($Z = \text{Si, Ge, Sn}$).¹⁴ As elucidated in Ref. 10, the change of the width of the gap can be traced back to two combined effects: (1) p - d hybridization, which obviously depends on the Zp states, and (2) their different lattice constants. From the PDOS of p states of the Z atom, as shown in Figs. 6–12, it is clear that the binding energy of p states of Z atoms decreases with increasing atomic number in a group and increases in a row, which seems quite well to illustrate the change of the gap as stated above. In fact, the effect of p - d hybridizations covers up the effect of lattice constant as the contraction or expansion of the lattice mainly has an influence on the delocalized p electrons but not to the already well localized d electrons of the transition metal. In order to further expound the influence of the lattice and the binding energy of p electrons, we also show the related data in Table I for the Mn_2CoSn compound with the lattice parameter of 5.80 Å, which is smaller than the experimental result. Clearly, it can be seen that the contraction of the lattice enlarges the energy gap. Compared with the Mn_2CoSi and Mn_2CoGe compounds with the equivalent lattice constant, it is also confirmed that the decreasing binding energy squeezes the energy gap.

TABLE II. The magnetic moment on atoms, calculated molecular magnetic moment M_C , and the experimental molecular magnetic moment M_E .

Composition Mn ₂ CoZ	Mn(B) (μ_B)	Mn(C) (μ_B)	Co (μ_B)	Z (μ_B)	M_C (μ_B)	M_E (μ_B)
Al	3.08	-1.98	0.92	-0.02	2.00	1.95
Ga	3.26	-2.16	0.90	0.00	2.00	1.98
In	3.54	-2.60	1.00	0.02	1.95	1.90
Si	3.12	-0.96	0.82	0.02	2.99	
Ge	3.14	-0.98	0.82	0.02	2.99	2.99
Sn	3.48	-1.54	0.94	0.04	2.99	2.98
Sb	3.20	-0.04	0.84	0.02	3.99	3.92

The spin-flip gaps (HM gap), the minimum energy required to flip a minority-spin electron from the valence band maximum edge to the majority-spin Fermi level, are the most proper indication of the half-metallicity of material. The detailed data have also been shown in Table I. It is clear that the HM gap shows a change with the atomic number similar to that of the band gap. However, a distinction can be observed by the comparison between the Mn₂CoSn with different lattice constants, that is, the contraction of the lattice decreases the HM gap, which is also observed in Co₂MnZ alloys and can be ascribed to the different Fermi level positions pinned in the band gap due to the rigid band shift with the change of lattice constant.

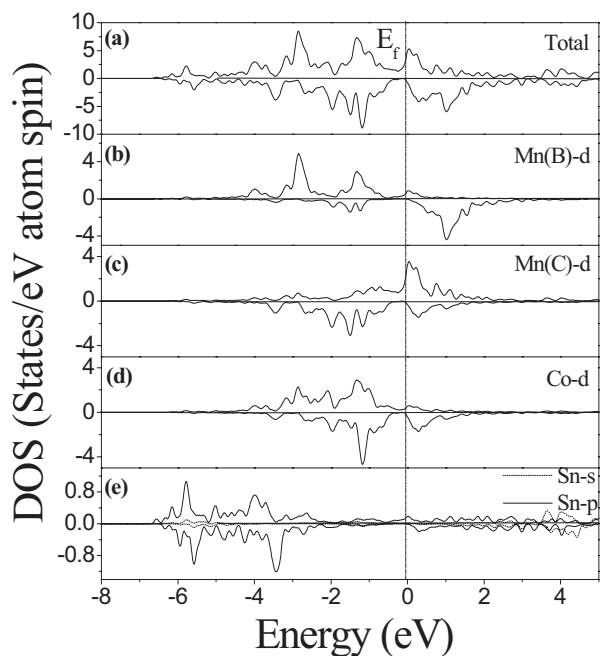


FIG. 11. Calculated spin-projected DOS plots for cubic Mn₂CoSn with the experimental lattice constant of 6.0688 Å. (a) The total DOS of Mn₂CoSn, (b) the partial DOS of the d component of Mn(B) atoms, (c) the partial DOS of the d component of Mn(C) atoms, (d) the partial DOS of the d component of Ni atoms, and (e) the partial DOS of s and p components of Sn atoms. The upper halves of each panel display the spin-up states and the lower halves the spin-down states.

D. Magnetic properties and Slater-Pauling rule

The preceding discussion is concerned with the band structure and the formation of the band gap. We now turn to the magnetic properties. The calculated and experimental magnetic moments for the compounds and for the single constituents are reported in Table II. The Mn(B) atom carries the largest moment (around 3 μ_B) in all the Mn₂CoZ compounds, which is similar to most of the Mn-based Heusler alloys. The Co atom has a positive moment of about 1 μ_B , which is similar to that in the full-Heusler Co₂MnZ alloys but different from that in semi-Heusler CoMnZ alloys. (At least, it is

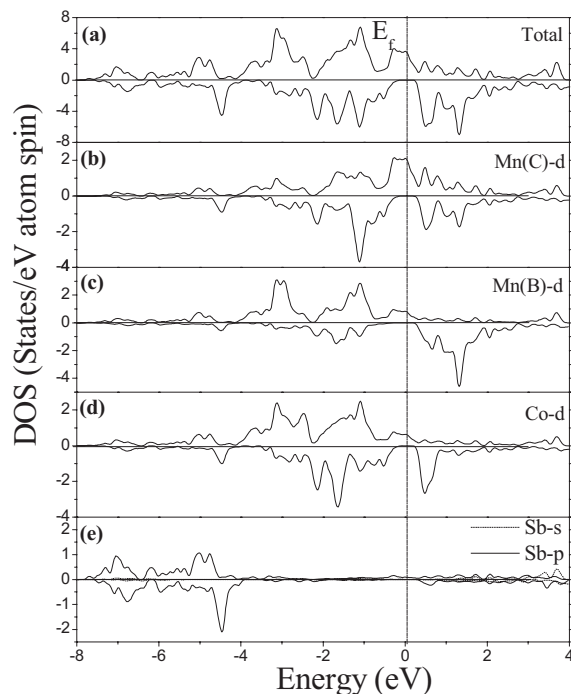


FIG. 12. Calculated spin-projected DOS plots for cubic Mn₂CoSb at the lattice constant of 5.8806 Å. (a) The total DOS of Mn₂CoSb, (b) the partial DOS of the d component of Mn(C) atoms, (c) the partial DOS of the d component of Mn(B) atoms, (d) the partial DOS of the d component of Co atoms, and (e) the partial DOS of s and p components of Sb atoms. The upper halves of each panel display the spin-up states and the lower halves the spin-down states.

well known that the magnetic moment of Co is antiferromagnetically aligned with respect to the Mn atom in semi-Heusler CoMnSb.⁹) We should pay more attention to the Mn(C) atom as it shows the most notable difference from the full-Heusler alloys with $L2_1$ structure and semi-Heusler alloys. The Mn(C) atom exhibits a varying magnetic moment with the different s - p atoms in the Mn_2CoZ alloys and couples antiferromagnetically to the Mn(B) and Co moments. Therefore, the total moments are $2 \mu_B$, $3 \mu_B$, and $4 \mu_B$ in the compounds with s - p elements of groups III, IV, and V, respectively, which are in good agreement with experimental values. It should also be pointed out that the integer value of the total magnetic moment is an indication of the half-metallic character.

It is known that in Heusler alloys, the ferromagnetic and antiferromagnetic moment alignments result from a competition between two physical mechanisms: the intra-atomic exchange splitting of the magnetic atom d states and the interatomic covalent interaction of d states.³⁶ The magnetic energy applies equally to the ferromagnetic and antiferromagnetic alignments, while the covalency mechanism benefits only the antiferromagnetic alignment. However, an intrinsic aspect of the covalency mechanism is a loss of local magnetization, which is the essence of the antiferromagnetic-ferromagnetic competition.^{10,36}

As shown in our previous report on the Mn_2NiGa with Hg_2CuTi structure, the Mn(C) atom is one of the nearest neighbors of the Mn(B) atom and has a small distance between them. So, we consider that there exists a strong direct interaction between their d states. Hence, the covalency mechanism is dominant to form the antiferromagnetic alignment between the Mn(C) moment and the Mn(B) moment. In order to further elucidate the character and action of Mn(C) in Mn_2CoZ compounds, as a typical example, we have compared Mn_2CoSb with Hg_2CuTi structure with semi-Heusler CoMnSb.^{9,13,38} In the case of the half-Heusler alloys, there is only one Co atom per unit cell and its d valence electrons hybridize with the Mn d valence electrons, creating an antiferromagnetic alignment. In the Mn_2CoZ alloys, the existence of the second Mn atom makes the physics of these systems more complex. The Mn(C) atom has a stronger hybridization with the Co atom than with the Mn(B) atom, which can be clearly observed from the PDOS shown in Figs. 6–12. So, as the second Mn is added, the reconstruction of the bands is mainly driven by hybridization between the Mn(C) d states and Co ones.

In the PDOS of Co d and Mn(C) d states, we can obviously observe a peak at about 0.5 eV above Fermi level for the minority-spin states in Mn_2CoZ alloys, which is not observed in the CoMnSb compound. So, this peak is completely induced by the Mn(C) atom. The occurrence of this peak decreases the minority-spin states of the Co atom below the Fermi level. As a consequence, the Co moment shows a positive moment of about $1 \mu_B$. It should also be noted that the Mn(C) atom has only a small magnetic moment in the Mn_2CoSb alloy. So, it is impossible that a strong exchange interaction between the Mn(C) and Co or Mn(B) atoms exists. Therefore, it can be concluded that the hybridization between the Mn(C) and Co atoms not only changed the mag-

nitude of magnetic moment of the Co atom but also dominated the sign of the Mn(B)-Co exchange interaction. Furthermore, associated with the compounds with large magnetic moment of Mn(C), we can believe that the Mn(B)-Co and Mn(B)-Mn(C) exchange interactions are the leading ones in Mn_2CoZ alloys, but the hybridization between the Mn(C) and Co atoms dominates the sign of the Mn(B)-Co exchange interaction. Usually, we think that the larger the magnetic moment, the stronger the exchange interaction. So, it is considered that the stronger Mn(B)-Co and Mn(B)-Mn(C) exchange interaction and the higher Curie temperature exist in the compounds with larger magnetic moment of Mn(C). The related work is being carried out. In addition, here, we must emphasize that the Mn(C) and Co are not nearest neighbors and their d electron energy is closely related to the p electron energy of the Z atom. So, we consider that the hybridization action of p electrons is necessary, although the Mn(C) and Co d states play the pivotal role to reconstruct the band structure change, the formation, and the coupling of magnetic moments.

As is well known, the half-metal Heusler alloys follow the Slater-Pauling rule. Many researchers focus on the alternative of the transition metal. Here, we want to investigate the behavior when we vary the valence of the s - p atom in the Mn_2CoZ alloy system with the special crystallized Hg_2CuTi structure. Half-metallic ferromagnets exhibit a gap in the minority density of states where the Fermi energy is pinned, which leads to the number of occupied minority states being an integer. Thus, the Slater-Pauling rule will be strictly fulfilled with $m_{HMF} = n_V - 6$ (n_V is the mean number of valence electrons per atom) for the spin magnetic moment per atom. In the case of four atoms per unit cell, as in full-Heusler compounds, one has to subtract 24 from the accumulated number of valence electrons N_V to find the spin magnetic moment M per unit cell: $M_H = N_V - 24$.³⁷

From Table II, one can clearly see that, as full-Heusler alloys with $L2_1$ structure, the Mn_2CoZ alloys also follow the $M_H = N_V - 24$ rule with varying Z atom. Furthermore, it was found that the spin magnetic moment M per unit cell increases with increasing valence concentration only by decreasing the magnetic moment of the antiparallel Mn(C) atom, while the magnetic moments of Mn(B) and Co are barely touched. Our interpretation is that the changes of the p electron number only have a strong influence on the magnetic moment of the Mn(C) atom. The reason is that the s - p atom that provides p electrons for the p - d hybridization is one of the nearest neighbors of Mn(C) and the Mn(C) atom has more empty bands in the majority-spin states, which makes it easier to seize electrons than the Co atom. So, from the PDOS of Mn(C) d states, as shown in Figs. 6–12, one can clearly see that the occupation degree of majority-spin bands of Mn(C) increases with increasing group number of s - p atom (e.g., along $In \rightarrow Sn \rightarrow Sb$) in the Periodic Table and the negative magnetic moment of Mn(C) becomes smaller and smaller. At the same time, we can also see that the energy of p electrons decreases and departs away from the energy where the d electron is mainly localized with increasing group number of s - p atom. This leads to the weakness of the s - p atom-mediated covalent interactions between Mn(C)

and Co, and the intra-atomic exchange interactions are popped out, that is, there are more bands in the majority-spin states of Mn(*C*) that are shifted and go below the Fermi level. Thus, although there are more occupied bands in the majority-spin states of Mn(*C*), the Fermi level is shifted slightly and remains to be pinned in the band gap of minority-spin states, which implies that the change of the number of *p* electrons does not destroy the half-metallicity.

IV. CONCLUSION

Using the FLAPW method, we have studied the Mn₂CoZ compounds with Hg₂CuTi-type structure. It is predicted that the compounds with Z=Al, Si, Ge, Sn, and Sb are half-metals. We find that there exist two mechanisms to induce the band gap (covalent band gap and *d-d* band gap) near the Fermi level in the minority-spin states. Only the *d-d* band gap determines the final width of the band gap, which is different in the two-Mn-contained compounds with conventional *L2*₁ structure and semi-Heusler alloys, where there is only one mechanism at work. The magnetic moment of Mn(*C*) is antiferromagnetically aligned to that of Mn(*B*) and Co. It is considered that the hybridization between the Mn(*C*) and Co atoms dominates the magnitude of magnetic moment of the Co atom and the sign of the Mn(*B*)-Co ex-

change interaction. As in conventional full-Heusler alloy, the Mn₂CoZ alloys follow the Slater-Pauling rule $M_H = N_V - 24$ with varying *Z* atom. However, the molecular magnetic moment M_H increases with increasing valence concentration only by decreasing the magnetic moment of the antiparallel Mn(*C*) atom, while the magnetic moments of Mn(*B*) and Co are untouched and the Fermi level is shifted slightly and remains to be pinned in the band gap of minority-spin states. Therefore, we predict that partly substituting one kind of *s-p* element for another will improve the other properties of the material but not destroy their half-metallicity. Experimentally, we successfully synthesized the Mn₂CoZ (Z = Al, Ga, In, Ge, Sn, Sb) compounds and confirmed that these compounds favor to form Hg₂CuTi-type structure instead of conventional *L2*₁ structure. In this structure, the two Mn atoms are nearest neighbors to each other and exhibit different magnetic characters. Therefore, we believe that it is the special crystallized structure that leads to a quite complex magnetic interaction and bring about many physical properties for the Mn₂Co-based alloys.

ACKNOWLEDGMENTS

This work was supported by the National Natural Science Foundation of China Grant No. 50671034 and the Natural Science Foundation of Hebei Grant No. E2006000063.

-
- ¹R. A. de Groot, F. M. Mueller, P. G. van Engen, and K. H. J. Buschow, Phys. Rev. Lett. **50**, 2024 (1983).
²G. A. Prinz, Science **282**, 1660 (1998).
³K. Ozdogan, I. Galanakis, E. Sasioglu, and B. Aktas, Solid State Commun. **142**, 492 (2007).
⁴H. van Leuken and R. A. de Groot, Phys. Rev. Lett. **74**, 1171 (1995).
⁵Warren E. Pickett, Phys. Rev. B **57**, 10613 (1998).
⁶J. H. Park, S. K. Kwon, and B. I. Min, Phys. Rev. B **65**, 174401 (2002).
⁷H. Akai and M. Ogura, Phys. Rev. Lett. **97**, 026401 (2006).
⁸F. Heusler, W. Starck, and E. Haupt, Verh. Dtsch. Phys. Ges. **5**, 220 (1903).
⁹I. Galanakis, P. H. Dederichs, and N. Papanikolaou, Phys. Rev. B **66**, 134428 (2002).
¹⁰J. Kübler, A. R. Williams, and C. B. Sommers, Phys. Rev. B **28**, 1745 (1983).
¹¹S. N. Holmes and M. Pepper, Appl. Phys. Lett. **81**, 1651 (2002).
¹²S. Fujii, S. Sugimura, S. Ishida, and S. Asano, J. Phys.: Condens. Matter **2**, 8583 (1990).
¹³S. Ishida, S. Fujii, S. Sugimura, and S. Asano, J. Phys. Soc. Jpn. **65**, 2152 (1995).
¹⁴S. Picozzi, A. Continenza, and A. J. Freeman, Phys. Rev. B **66**, 094421 (2002).
¹⁵K. H. J. Buschow and P. G. van Engern, J. Magn. Magn. Mater. **25**, 90 (1981).
¹⁶R. Weht and W. E. Pickett, Phys. Rev. B **60**, 13006 (1999).
¹⁷C. Jiang, M. Venkatesan, and J. M. D. Coey, Solid State Commun. **118**, 513 (2001).
¹⁸K. Ozdogan, I. Galanakis, E. Sasioglu, and B. Aktas, J. Phys.: Condens. Matter **18**, 2905 (2006).
¹⁹K. Ozdogan, I. Galanakis, E. Sasioglu, and B. Aktas, Phys. Status Solidi (RRL) **1**, 95 (2007).
²⁰I. Galanakis, K. Ozdogan, E. Sasioglu, and B. Aktas, Phys. Rev. B **75**, 092407 (2007).
²¹P. J. Webster, Contemp. Phys. **10**, 559 (1969).
²²C. C. M. Campbell, J. Phys. F: Met. Phys. **5**, 1931 (1975).
²³R. B. Helmholtz and K. H. J. Buschow, J. Less-Common Met. **128**, 167 (1987).
²⁴G. D. Liu, X. F. Dai, S. Y. Yu, Z. Y. Zhu, J. L. Chen, G. H. Wu, H. Zhu, and J. Q. Xiao, Phys. Rev. B **74**, 054435 (2006).
²⁵X. F. Dai, G. D. Liu, L. J. Chen, J. L. Chen, and G. H. Wu, Solid State Commun. **140**, 533 (2006).
²⁶E. Wimmer, H. Krakauer, M. Weinert, and A. J. Freeman, Phys. Rev. B **24**, 864 (1981).
²⁷M. Weinert, E. Wimmer, and A. J. Freeman, Phys. Rev. B **26**, 4571 (1982).
²⁸J. Rath and A. J. Freeman, Phys. Rev. B **11**, 2109 (1975).
²⁹P. E. Blochl, O. Jepsen, and O. K. Andersen, Phys. Rev. B **49**, 16223 (1994).
³⁰M. P. Raphael, B. Ravel, Q. Huang, M. A. Willard, S. F. Cheng, B. N. Das, R. M. Stroud, K. M. Bussmann, J. H. Claassen, and V. G. Harris, Phys. Rev. B **66**, 104429 (2002).
³¹T. J. Burch, T. Litrenta, and J. I. Budnick, Phys. Rev. Lett. **33**, 421 (1974).
³²M. Pugaczowa-Michalska, A. Go, L. Dobrzynski, and S. Lipinski, J. Magn. Magn. Mater. **256**, 46 (2003).

- ³³C. M. Fang, G. A. de Wijs, and R. A. de Groot, *J. Appl. Phys.* **91**, 8340 (2002).
- ³⁴I. Galanakis, P. H. Dederichs, and N. Papanikolaou, *Phys. Rev. B* **66**, 174429 (2002).
- ³⁵S. Fujii, S. Ishida, and S. Asano, *J. Phys. Soc. Jpn.* **64**, 185 (1995).
- ³⁶A. R. Williams, R. Zeller, V. L. Moruzzi, C. D. Gelatt, and J. Kubler, *J. Appl. Phys.* **52**, 2067 (1981).
- ³⁷G. H. Fecher, H. C. Kandpal, S. Wurmehl, C. Felser, and G. Schönhense, *J. Appl. Phys.* **99**, 08J106 (2006).
- ³⁸E. Sasioglu, L. M. Sandratskii, P. Bruno, and I. Galanakis, *Phys. Rev. B* **72**, 184415 (2005).